First-principles study of NO oxidation on $Pt/CaTiO_3$ interface

Huailong Li [a,b], Xiangmei Duan [b], Yange Suo [a], Qiuju Zhang [a,*], Liang Chen [a,*]

[a] Ningbo Institute of Materials Technology and Engineering, Chinese Academy of Sciences, Ningbo 315201, Zhejiang, PR China
[b] Faculty of Science, Ningbo University, Ningbo 315211, Zhejiang, PR China

Keywords:
NO oxidation
$CaTiO_3$
NO_2 desorption
First-principles
Automobile exhaust-gas catalyst

A B S T R A C T

A well-dispersed noble metal on perovskite support is expected to show good catalytic ability for NO oxidation under oxygen-rich conditions, which is an important step in reducing NO in lean burn exhaust gas. In this study, we investigated the catalytic oxidation of NO to NO_2 on a $Pt_4/CaTiO_3$ (001) model to evaluate interfacial effect. Results showed that O_2 preferred Pt–Ti interface sites, and that the decomposition of O_2 required a dissociation activation barrier of 0.97 eV. The decomposed O–O on the interface required nearly no activation barrier in the subsequent NO oxidation. However, the most rate-limiting step involved the desorption of the second formed NO_2 from interfacial $Pt_4/CaTiO_3$ (001), which yielded a significant desorption barrier of 2.63 eV. These findings can help understand the oxidation process of NO to NO_2 on noble-metal–perovskite interface.

1. Introduction

NO_x emission in lean burn and diesel exhaust is one of the main sources of air pollution. Although efficient in converting toxic gases from gasoline engines, three-way catalysts are generally ineffective in reducing NO_x in diesel engine under oxygen-rich conditions [1,2]. Therefore, developing NO_x storage reduction (NSR) catalysts consisting of a precious metal supported on metal oxides [3] has become an alternative technology for reducing NO_x emission [4]. The presence of a precious metal is critical in NO oxidation under oxygen-rich condition [5], which is an important step in NO_x storage. NO oxidation by excessive O_2 can occur in the presence of noble metals [6]. However, an important drawback of traditional precious metal support involves the aggregation of supported noble metals, which directly leads to catalyst invalidation.

To maintain catalytic activity, various studies were conducted to find a more appropriate support for good dispersion of the noble metal [6,7]. Several perovskites such as $CaTiO_3$ and $LaFeO_3$ are recently found to be capable of preventing the aggregation of supported Pt or Pd particles by refreshing them in and out of the perovskite lattice. Pt-doped $CaTiO_3$ or Pd-doped $LaFeO_3$ materials are known as "intelligent catalysts" [2,8,9], and are expected to efficiently save the limited precious metal resources. However, the inherent electronic nature of the interface between the noble metal and perovskite has not been well studied. For instance, how the metal support interface affects the catalytic process of NO_x remains unclear.

Given that the oxidation of NO to NO_2 is the most important step for reducing NO in lean burn exhaust gas [10,11], we studied the catalytic oxidation of NO on a metal support interface based on a $Pt_4/CaTiO_3$ model. First, the effects of cluster size of Pt_n (n = 4, 5, and 6) on the support was evaluated by analyzing interfacial electronic character and binding energies. Subsequently, the adsorption and dissociation of O_2 on $Pt_4/CaTiO_3$ were investigated to determine the activation barrier and the most favorable sites for active dissociated O atoms. After producing active O atoms, the catalytic reaction process of $2NO + O_2 \rightarrow 2NO_2$ on Pt_4 and the interface were compared to evaluate the $Pt_4/CaTiO_3$ interfacial effect. Finally, we mapped out the energy landscape of NO_2 desorption and found that refreshing the $Pt_4/CaTiO_3$ catalyst is an important and rate-limiting step for the entire NO-oxidation process.

2. Computational methods

All calculations were performed based on the density functional theory (DFT) using the Vienna ab initio simulation package (VASP) [12,13]. The electron–ion interactions were treated by all-electron projector augmented wave (PAW) approximation [14,15]. Electronic exchange–correlation energies were determined by Perdew, Burke, and Enzer (PBE) [16] functional within spin-polarized generalized gradient approximation (GGA) [17]. Climbing image nudged elastic band (cNEB) method [18,19] was used to calculate the activation energies of O_2 dissociation and NO oxidation.

* Corresponding authors.
E-mail addresses: zhangqj@nimte.ac.cn (Q. Zhang), cnchenliang@nimte.ac.cn (L. Chen).

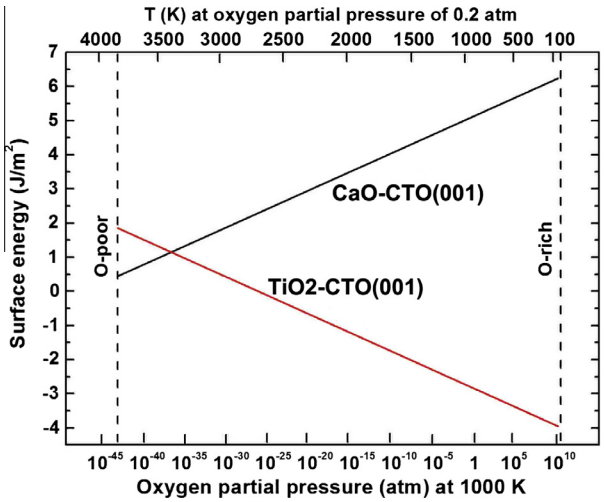

Fig. 1. The calculated surface energy comparison of CaO and TiO_2 terminated $CaTiO_3$(001) surface, denoted as CaO–CTO(001) and TiO_2–CTO(001), in O_2-rich and O_2-poor conditions at temperature of 1000 K.

A cutoff energy of 350 eV for the plane wave basis and a Monkhorst–Pack set [20] of $2 \times 2 \times 1$ *k*-points were set in the entire calculations. Two terminated $CaTiO_3$ (001) surfaces (i.e., TiO_2- and CaO-terminated surfaces) were built with a 2×2 periodic supercell. The lattice constants of bulk $CaTiO_3$ were calculated to be $a = 5.464$ Å, $b = 5.480$ Å, and $c = 7.452$ Å, which agree well with $a = 5.290$ Å, $b = 5.412$ Å, and $c = 7.537$ Å in the reference [21]. Both supercells contain five-layer slabs and a 15 Å vacuum space that is perpendicular to the surface. All atoms were fully relaxed with the ionic forces converging to 0.03 eV/Å and total energy to 10^{-4} eV/Å. To ensure that five-layer model is sufficient to converge adsorption energies ($E_{ads} = (E_{NO/Pt/TiO2} - E_{Pt/TiO2} - E_{NO})$), we compared the E_{ads} of NO adsorption on five-layer and seven-layer $CaTiO_3$(001) models and found that the difference is only 0.01 eV to 0.02 eV. We gave particular attention to the TiO_2 (001) terminated model in this study, because we are interested in the oxidation of NO under excessive O_2 conditions, and the surface energy of the TiO_2 (001)-terminated model is found to be lower than that of CaO (001) under O_2-rich conditions (see Fig. 1).

3. Results and discussion

3.1. $Pt_n/CaTiO_3$

To select a suitable and computationally affordable Pt cluster to deposit on the $CaTiO_3$ surface, we first compared the different isomers and cohesive energies (E_c) of three Pt_n ($n = 4, 5, 6$) clusters. E_c was calculated as $E_c = E_{Ptn}/n$ to identify the most favorable Pt_n cluster isomers. For $n = 4$, among the optimized linear 1D, square 2D, and tetrahedral 3D clusters, the tetrahedral Pt_4 cluster with $E_c = 3.28$ eV was found to be the most stable isomer. For the Pt_5 cluster, the trigonal bipyramid shows the largest E_c of 3.51 eV in comparison with the square pyramid and 2D pentagon isomers. When *n* is increased to 6, the 2D double square becomes the most stable isomer, with the largest E_c of 3.74 eV. The calculated bond lengths of Pt–Pt are 2.598 Å in Pt_4, 2.633 Å in Pt_5, and 2.422 Å in Pt_6 in their favorable isomers, which are all shorter than 2.775 Å of Pt–Pt bond in the previously calculated Pt_4 cluster [22].

When a Pt_n cluster is deposited on TiO_2- or CaO-terminated (001) surface, significant deformation or even transformation occurs for the most stable Pt_5 and Pt_6 isomers. Formation energy (E_f) was calculated as $E_f = (E_{Ptn/TiO} - E_{TiO} - E_{Ptn})/n$. Therefore, we selected and placed the most stable Pt_4 tetrahedral cluster onto the $CaTiO_3$(001) surface, which results in $E_f = 1.04$ eV. To find the most stable metal support site, three adstructures with Pt_4 cluster vertex, bridge, and planar binding were constructed and compared. Similar to our previous study on Pd_4/MOF-5 [23], the most favorable interfacial structure was found for the planar contact model, as shown in Fig. 2. The three bottom Pt atoms bind with three O atoms and two Ti atoms of the six-member Ti–O–Ti ring on the TiO_2-terminated surface with a d_{Pt-O} of about 2.07 Å. On the CaO-terminated surface, three Pt atoms bind to three Ti atoms with a d_{Pt-Ti} of about 2.73 Å. The corresponding adhesion energies ($E_{adh} = E_{Pt4/CaTiO3} - E_{Pt4} - E_{CaTiO3}$) are calculated to be −4.16 and −6.02 eV, respectively. The higher E_{adh} of the Pt_4/CaO model is possibly ascribed to the different electron characters in these two surfaces.

To understand the electronic nature of Pt_4/TiO_2 and Pt_4/CaO interfaces, we calculated electron density difference (EDD) between the adstructures and separate components with each atom frozen at their optimized positions [24]. Our previous study has indicated that CaO and TiO_2-terminated surfaces displayed distinct electronic features, i.e., electron-rich (−0.30 |e|) and electron-poor (+0.73 |e|) character, respectively [25]. Similarly, such trend was also found in the $Pt_4/CaTiO_3$ interface. Bader charge analysis indicates that the Pt_4 cluster donates approximately 0.05 |e| to the electron-poor TiO_2-terminated substrate while gaining 0.63 |e| from the electron-deficit CaO-terminated substrate. On the $Pt_4/TiO_{2\text{-term}}$ interface, the top Pt gains 0.21 |e|, whereas the other three bottom Pt atoms lose 0.26 |e| in total, leading to a net 0.05 |e| transferred from Pt_4 to the TiO_2-terminated surface. As shown in Fig. 2e, the blue area around the three bottom Pt atoms displays the electron-donation character. In contrast, the Pt_4 cluster gains 0.63 |e| from the CaO-terminated substrate, similar to −0.55 |e| of Pt/$CaO_{\text{-term.}}$ interface [25]. This result can be attributed to the electron-rich feature of the CaO-terminated surface enabling the surface to lose extra electrons to bind the Pt_4 cluster. Notably in EDD (Fig. 2f), electron accumulation (red area) takes place around Pt atoms, showing the electron transfer from the $TiO_{2\text{-term}}$ surface to Pt_4 clusters.

3.2. Adsorption of NO on $Pt_4/CaTiO_3$

The analysis above indicates that metal support interactions lead to different electron redistributions of the four Pt atoms. Hence, we next studied how Pt_4 deposition influences the oxidation behavior of NO. For NO adsorption on $Pt_4/CaTiO_3$, two adsorption sites through N or O ends were taken into account to locate the most favorable adsorption sites. Similar to results of the previous study [26,27], adsorption through the N end is found to be more favorable than through the O end. As shown in Fig. 3, three different adsorption structures, including top binding (top-NO), Pt–Pt bridge binding (bridge-NO), and Pt–Ti interface binding (interface-NO), were considered, and the corresponding adsorption energies ($E_{ads} = E_{total} - E_{molecule} - E_{surface}$) and geometry parameters are summarized in Table 1.

For onefold adsorption (i.e., NO interacting with only one Pt atom), the top Pt atom shows stronger affinity toward NO than the bottom Pt atoms, which is possibly ascribed to the difference in electron redistribution between top and bottom Pt atoms. The relatively electron-rich top Pt atom could donate electrons to NO, yielding stronger top-NO adstructure (Fig. 3a). In this structure, the bond length of Pt–N (d_{Pt-N}) is calculated to be 1.795 Å, which is significantly shorter than the d_{Pt-N} of about 1.837 Å for NO adsorption on Pt(111) top site [28]. In twofold adsorption, the N atom can bind with two adjacent Pt atoms on the Pt_4 cluster, or with Pt and Ti atoms on the interface (see Fig. 3b and c). The bridged Pt–Pt form two asymmetric Pt–N bonds of 1.923 and

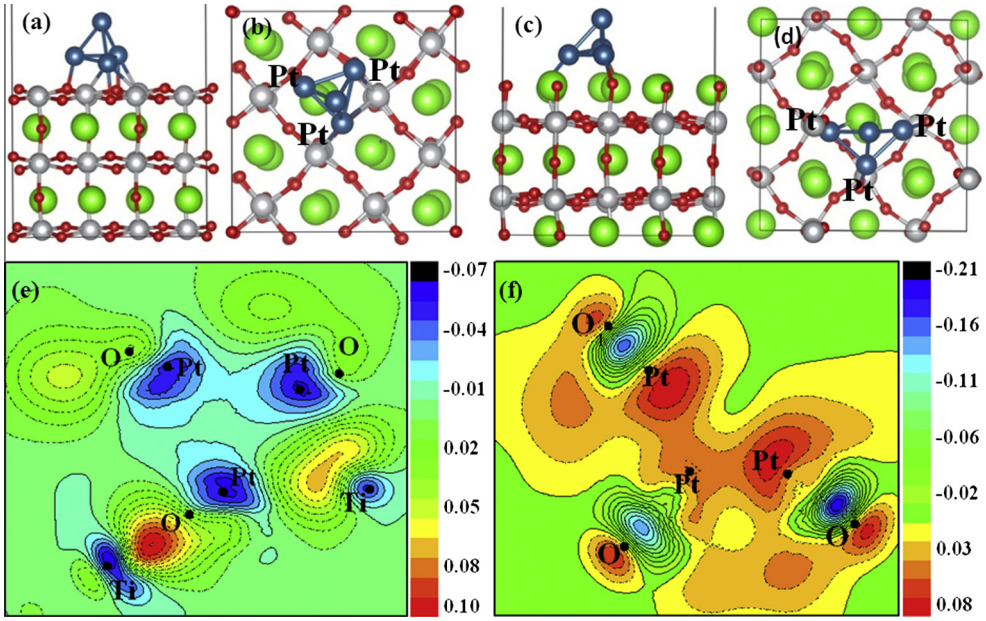

Fig. 2. (a) and (c) are the side view of Pt_4 deposition onto TiO_2- and CaO-terminated $CaTiO_3(001)$ surfaces; (b) and (d) are the corresponding top-view structures of $Pt_4/CaTiO_3(001)$; (e) and (f) present the charge density difference (EDD) of Pt_4/TiO_2 terminated (001) and Pt_4/CaO terminated (001) surfaces. Ca, O, Ti and Pt atoms are represented in green, red, gray, and dark-green, respectively. (For interpretation of the references to color in this figure legend, the reader is referred to the web version of this article.)

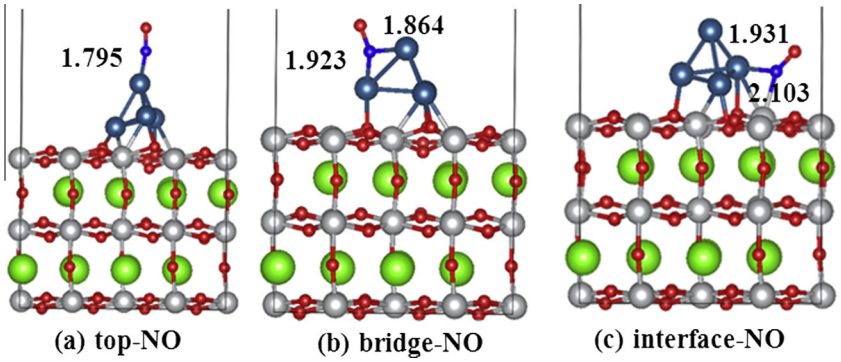

Fig. 3. Three possible adstructures of NO adsorption on top Pt, bridge Pt–Pt bond and interface Pt–Ti bond of $Pt_4/TiO_2(001)$ termination, to form (a) top-NO, (b) bridge-NO and (c) interface-NO states, respectively. N atom is represented in blue ball. The unit of distance is Å.

Table 1
The calculated adsorption energies (E_{ads}) and geometrical parameters of NO and O_2 adsorption on Pt_4/TiO_2 terminated (001) surface. (Unit of distance in Å, angle in degree and energy in eV).

Adsorption site	E_{ads}	d_{Pt-N}	d_{Ti-N}	d_{N-O}	∠O–N–Pt
NO				1.225	
Top-NO	−2.94	1.795		1.243	156.7
Bridge-NO	−3.00	1.923		1.281	140.6
		1.864			
Interface-NO	−3.06	2.103	1.931	1.218	126.9
Adsorption site	E_{ads}	d_{Pt-O}	d_{Ti-O}	d_{O-O}	∠O–O–Pt
O_2				1.293	
Top-O_2	−1.90	2.172		1.403	77.7
		1.983			
Bottom-O_2	−1.87	1.981		1.364	111.8
Bridge-O_2	−2.09	1.948		1.432	107.5
		2.107			
Interface-O_2	−2.40	1.931	1.933	1.437	115.2

1.864 Å, yielding an ∠O–N–Pt of 140.6° and a slightly higher E_{ads} of 3.00 eV in comparison with top-NO adstructure. In the case of Pt–Ti interface binding, the N atom binds with both Pt and Ti with d_{Pt-N} and d_{Ti-N} of 2.103 and 1.910 Å, forming a ∠O–N–Ti bend angle of 141.6°. The resulting largest E_{ads} = 3.06 eV indicates that this structure is the most favorable stable one.

To further analyze the electron transfer, Bader charge analysis was conducted to show that electron transfer from $Pt_4/CaTiO_3$ to NO was in the range of 0.42 |e| to 0.58 |e| in these three configurations, implying a strong chemical binding nature. In addition, simultaneous N and O binding with Pt were also considered at the top Pt site and interfacial Pt–Ti site. However, such binding modes are unstable compared with the three binding modes above.

3.3. O_2 adsorption and dissociation on $Pt_4/CaTiO_3$

O_2 adsorption on $Pt_4/CaTiO_3$ displays a similar trend to NO adsorption. Among the above-mentioned adsorption sites, Pt–Ti interfacial adsorption (interface-O_2) also results in the highest E_{ads} = 2.40 eV (Fig. 4d). In this adstructure, two symmetric bonds ($d_{O-Pt} = d_{O-Ti}$ = 1.93 Å) are formed, accompanied by the largest electron transfer (0.83 |e|) from Pt and Ti atoms to O_2. In contrast, the lowest E_{ads} (1.87 eV) is found for onefold adsorption on the bottom Pt site.

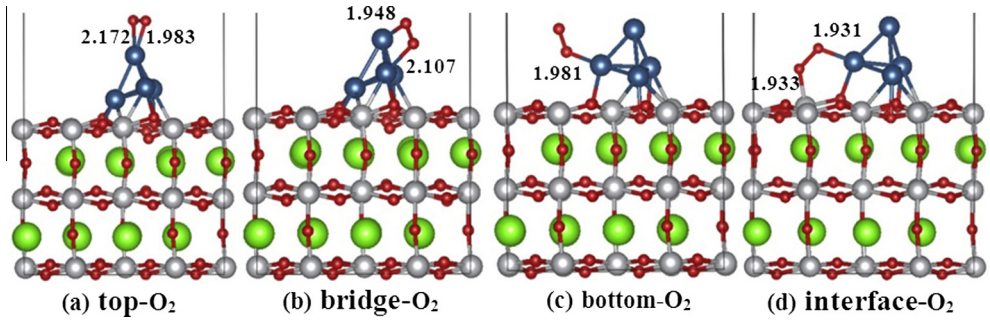

Fig. 4. The possibly adsorption states of (a) top-O_2, (b) bridge-O_2, (c) bottom-O_2 and (d) interface-O_2, formed by O_2 adsorption on top Pt, bridge Pt–Pt bond, bottom Pt and interface Pt–Ti bond adsorption sites of Pt_4/TiO_2 terminated (001) surface, respectively.

We next investigated how O_2 is dissociated on the interface to produce active oxygen atoms. Top-O_2 and bridge-O_2 adsorption was observed to yield the same adstructures for dissociated O atoms. In contrast, the bottom Pt adsorption site yields a full-binding O atom, i.e., each dissociated O atom form two bonds. Hence, only two adstructures of dissociated O atoms were finally considered for evaluating the dissociation ability of O_2 following paths I and II, as displayed in Fig. 5. In the plotted path I, the O–O bond length is gradually elongated from 1.43 Å in the initial bridge-O_2 (E_{ads} = 2.27 eV) to 1.82 Å in the transition state (TS^I). The increasing O–O distance results in an activation barrier of 0.53 eV, which is slightly smaller than the calculated barrier (0.62 eV) of O_2 dissociation on Pt(111) [29]. In the final dissociated state, the two active O atoms are completely separated by 5.05 Å. These two separated O atoms bind with Pt and one surface Ti atom, respectively, yielding an E_{ads} of 3.97 eV. In path II, O_2 dissociation can possibly occur from the initial interface Pt–Ti adstructure. As shown in Fig. 5b, the initial O–O bond on the Pt–Ti interface is 1.44 Å, and is gradually broken to be 2.40 Å in TS^{II}, resulting in an activation barrier of 0.97 eV. Upon complete dissociation, the two isolated active O atoms bind with Pt and Ti by enlarging the Pt–O and Ti–O bonds to 1.86 and 1.66 Å, respectively, producing an E_{ads} of 2.28 eV. The lower E_{ads} of dissociated O atoms on the Pt–Ti interface is expected to provide more active O atoms to oxidize NO, although the Pt–Ti interface in path II requires higher O_2 dissociation barrier (0.97 eV) than that of bridge-O_2 dissociation (0.53 eV).

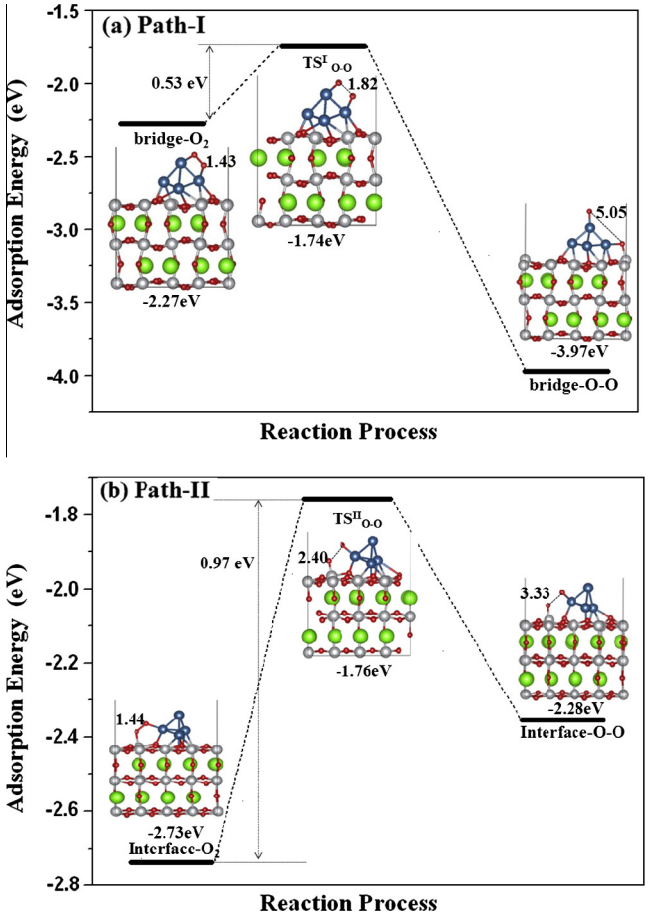

Fig. 5. The two possible reaction channels of O_2 decomposition on bridge Pt–Pt bond and Pt–Ti interface of $Pt_4/TiO_2(001)$ termination to produce active O atoms, as plotted in (a) path-I and (b) path-II, respectively. The distance unit is Å.

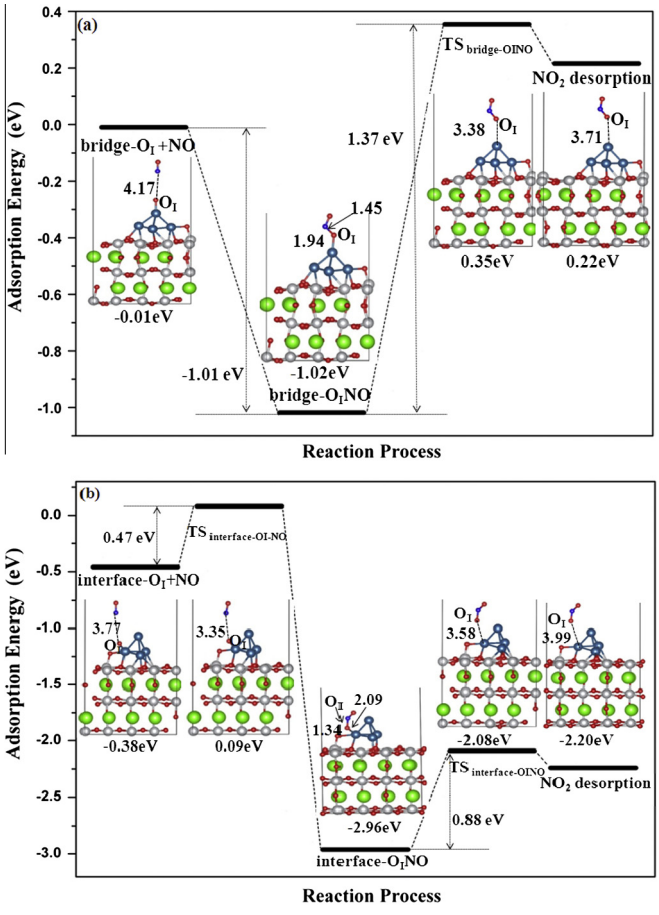

Fig. 6. The whole reaction processes combined with the first NO oxidation on O_I atom and the subsequent NO_2 desorption, occurred on (a) bridge Pt–Pt bond and (b) Pt–Ti interface of $Pt_4/TiO_2(001)$ termination. The distance unit is Å.

3.4. First NO oxidation and desorption

In principle, catalysts should remain clean after completing the catalyzed reactions. Therefore, we next investigated the reaction process of NO oxidation and the subsequent NO_2 desorption from the $Pt_4/CaTiO_3$ surface. The first NO oxidation reactions occurring on the dissociated bridge–O_I and interface–O_I atoms are mapped out in Fig. 6. As shown in Fig. 6(a), the O_I atom of the dissociated bridge–O_2 oxidizes the first approaching NO without no activation barrier. The produced NO_2 is bound on the top Pt, with E_{ads} of 1.02 eV and $\angle O_I$–N–O of 109.0°. The O_I–Pt bond is elongated from the original 1.76 Å to 1.94 Å. Upon the breakage of the O_I–Pt bond, NO_2 desorbs from the Pt_4 cluster by increasing the distance to 3.38 Å in the $TS_{bridge-OINO}$. The desorption barrier is 1.37 eV. As far as the first NO oxidation on O_I of Pt–Ti interface is concerned, a more favorable reaction process is obviously noticed in Fig. 6(b). Although the NO oxidation barrier of 0.47 eV is larger than that of the bridge-O_I, the following NO_2 desorption requires only 0.88 eV for the gas to leave the interfacial Pt–Ti bond. Combined with the NO oxidation and desorption process, the whole reaction energy in the interfacial O_I oxidation is favorable because of its exothermic energy of 1.82 eV.

3.5. Second NO oxidation and desorption

As plotted in Fig. 7, although the initial oxidation step occurs virtually without barrier, the second NO oxidation and desorption on both bridge-O_{II} and interfacial-O_{II} lead to more difficult processes. The subsequent second NO_2 desorption is the rate-limiting step, with the activation barrier of 1.66 and 2.63 eV, respectively. In Fig. 7(a), the second NO oxidation elongates the O_{II}–Pt bond from 1.81 Å to 2.05 Å and results in an E_{ads} of 0.91 eV. The formed NO_2 is bent with $\angle O_{II}$–N–O = 109.5°. To refresh the catalyst $Pt_4/CaTiO_3$, the activation barrier of 1.66 eV should leave the NO_2 molecule free. In comparison, the second NO_2 desorption on interfacial Pt–Ti leads to a larger activation barrier of 2.63 eV but a slightly lower E_{ads} (1.14 eV) for NO_2 formation, as shown in Fig. 7(b). Overall, the second NO reactions on bridge-O_{II} and interfacial-O_{II} are both endothermic, with 1.3 and 0.8 eV, indicating that the second NO_2 is more unfavorably desorbed, hence rendering this process as the most energy-consuming step.

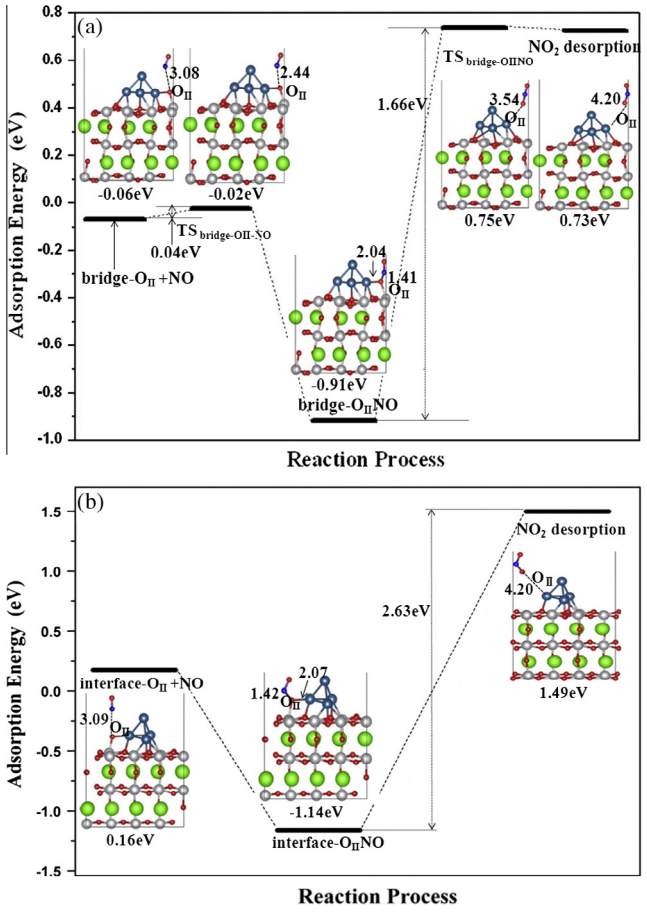

Fig. 7. The most rate-limiting step of the second NO oxidation on O_{II} and the subsequent NO_2 desorption from $Pt_4/TiO_2(001)$ termination. (a) and (b) refer to the reaction on bridge Pt–Pt and Pt–Ti interface, respectively. The distance unit is Å.

4. Conclusion

NO oxidation on a perovskite-supported Pt_4 cluster was investigated based on first-principles DFT calculations. Bader charge analysis and EDD show that, when interacting with the Pt_4 cluster, CaO- and TiO_2-terminated $CaTiO_3$ (001) surfaces act as electron donor and acceptor, respectively. The calculated dissociation barriers of O–O decomposition on bridge Pt–Pt and interface Pt–Ti correspond to 0.53 and 0.97 eV. The subsequent NO oxidation on the active O readily occurs because of their small reaction barriers of less than 0.47 eV. For the entire reaction, the second NO_2 desorption from $Pt_4/CaTiO_3$ is the most energy-consuming step, because the desorption barrier on bridge and interface sites are 1.66 and 2.63 eV, respectively. We expect that our study is helpful for understanding the NO oxidation mechanism on well-dispersed perovskite-supported noble metal clusters.

Acknowledgments

We gratefully acknowledge the financial support of the National Key Basic Research Program of China (Grant No. 2013CB934800), the National Science Foundation of China (Grant No. 51472254), and the Ningbo NSF (2014A610112 and 2012A610117).

Reference

[1] N. Takahashi, H. Shinjoh, T. Iijima, T. Suzuki, K. Yamazaki, K. Yokota, H. Suzuki, N. Miyoshi, S.I. Matsumoto, T. Tanizawa, T. Tanaka, S.S. Tateishi, K. Kasahara, The new concept 3-way catalyst for automotive lean-burn engine: NO_x storage and reduction catalyst, Catal. Today 27 (1996) 63–69.

[2] Z. Say, M. Dogac, E.I. Vovk, Y.E. Kalay, C.H. Kim, W. Li, E. Ozensoy, Palladium doped perovskite-based NO oxidation catalysts: The role of Pd and B-sites for NO_x adsorption behavior via in-situ spectroscopy, Appl. Catal. B: Environ. 154–155 (2014) 51–61.

[3] G. Liu, P.X. Gao, A review of NO_x storage/reduction catalysts: mechanism, materials and degradation studies, Catal. Sci. Technol. 1 (2011) 552–568.

[4] Q.Q. Zhang, L.F. Lv, J.X. Zhu, X.Q. Wang, J. Wang, M.Q. Shen, The effect of CO on NO reduction over Pt/Pd-based NSR catalysts at low temperature, Catal. Sci. Technol. 3 (2013) 1069–1077.

[5] C.H. Kim, G.S. Qi, K. Dahlberg, W. Li, Strontium-doped perovskites rival platinum catalysts for treating NO_x in simulated diesel exhaust, Science 327 (2010) 1624–1627.

[6] S. Roy, A. Baiker, NO_x storage-reduction catalysis: from mechanism and materials properties to storage-reduction performance, Chem. Rev. 109 (2009) 4054–4091.

[7] H. Tanaka, M. Taniguchi, M. Uenishi, N. Kajita, I. Tan, Y. Nishihata, J. Mizuki, K. Narita, M. Kimura, K. Kaneko, Self-regenerating Rh- and Pt-based perovskite catalysts for automotive-emissions control, Angew. Chem. Int. Edit. 45 (2006) 5998–6002.

[8] Y. Nishihata, J. Mizuki, T. Akao, H. Tanaka, M. Uenishi, M. Kimura, T. Okamoto, N. Hamada, Self-regeneration of a Pd-perovskite catalyst for automotive emissions control, Nature 418 (2002) 164–167.

[9] X.Y. Wang, X.X. Qi, Z.L. Chen, L.L. Jiang, R.H. Wang, K.M. Wei, Studies on SO_2 tolerance and regeneration over perovskite-type $LaCo_{1-x}PtxO_3$ in NO_x storage and reduction, J. Phys. Chem. C 118 (2014) 13743–13751.

[10] V.I. Pârvulescu, P. Grange, B. Delmon, Catalytic removal of NO, Catal. Today 46 (1998) 233–316.

[11] L.C. José, Fajín, M. Natália, D.S. Cordeiro, José R.B. Gomes, DFT study on the reaction of NO oxidation on a stepped gold surface, Appl. Catal. A: Gen. 379 (2010) 111–120.
[12] G. Kresse, J. Furthmüller, Efficiency of ab-initio total energy calculations for metals and semiconductors using a plane-wave basis set, Comp. Mater. Sci. 6 (1996) 15–50.
[13] G. Kresse, J. Hafner, Ab initio molecular dynamics for open-shell transition metals, Phys. Rev. B 48 (1993) 13115–13118.
[14] P.E. Blöchl, Projector augmented-wave method, Phys. Rev. B 50 (1994) 17953–17979.
[15] G. Kresse, D. Joubert, From ultrasoft pseudopotentials to the projector augmented-wave method, Phys. Rev. B 59 (1999) 1758–1775.
[16] J.P. Perdew, K. Burke, M. Ernzerhof, Generalized gradient approximation made simple, Phys. Rev. Lett. 77 (1996) 3865–3868.
[17] J.P. Perdew, J.A. Chevary, S.H. Vosko, K.A. Jackson, M.R. Pederson, D.J. Singh, C. Fiolhais, Atoms, molecules, solids, and surfaces: applications of the generalized gradient approximation for exchange and correlation, Phys. Rev. B 46 (1992) 6671–6687.
[18] G. Henkelman, B.P. Uberuaga, H. Jónsson, A climbing image nudged elastic band method for finding saddle points and minimum energy paths, J. Chem. Phys. 113 (2000) 9901–9904.
[19] G. Henkelman, H. Jónsson, Improved tangent estimate in the nudged elastic band method for finding minimum energy paths and saddle points, J. Chem. Phys. 113 (2000) 9978–9985.
[20] H.J. Monkhorst, J.D. Pack, Special points for Brillouin-zone integrations, Phys. Rev. B 13 (1976) 5188–5192.
[21] E. Cockayne, B.P. Burton, Phonons and static dielectric constant in $CaTiO_3$ from first principles, Phys. Rev. B 62 (2000) 3735–3743.
[22] R.L.T. Parreira, G.F. Caramori, S.E. Galembeck, F. Huguenin, The Nature of the Interactions between Pt4 Cluster and the Adsorbates $^{\cdot}H$, $^{\cdot}OH$, and H2O, J. Phys. Chem. A 112 (2008) 11731–11743.
[23] T.Y. Wang, Q.J. Zhang, B.H. Li, H. Chen, L. Chen, Density functional study of hydrogen spillover on direct Pd-doped metal-organic frameworks IRMOF-1, Int. J. Hydrogen Energy 37 (2012) 5081–5089.
[24] R.I. Eglitis, D. Vanderbilt, Ab initio calculations of the atomic and electronic structure of $CaTiO_3$ (001) and (011) surfaces, Phys. Rev. B 78 (2008) 155420.
[25] Q.J. Zhang, B.H. Li, H.Y. Wang, Y.G. Suo, L. Chen, A first-principles study of CO oxidation by surface oxygen on Pt-incorporated perovskite catalyst ($CaPt_xTi_{1-x}O_3$), RSC Adv. 4 (2014) 30530–30535.
[26] H. Aizawa, Y. Morikawa, S. Tsuneyuki, K. Fukutani, T. Ohno, A density-functional study of the atomic structures and vibrational spectra of NO/Pt(111), Surf. Sci. 514 (2002) 394–403.
[27] F. Garin, Mechanism of NO_x decomposition, Appl. Catal. A: Gen. 222 (2001) 183–219.
[28] W.A. Brown, D.A. King, NO chemisorption and reactions on metal surfaces: a new perspective, J. Phys. Chem. B 104 (2000) 2578–2595.
[29] J.M.M. de la Hoz, P.B. Balbuena, Geometric and electronic confinement effects on catalysis, J. Phys. Chem. C 115 (2011) 21324–21333.